

# Sinogram Denoising of Cryo-Electron Microscopy Images

Taneli Mielikäinen<sup>1</sup> and Janne Ravantti<sup>2</sup>

<sup>1</sup> HIIT Basic Research Unit  
Department of Computer Science  
University of Helsinki, Finland  
`tmielika@cs.Helsinki.FI`

<sup>2</sup> Institute of Biotechnology and  
Faculty of Biosciences  
University of Helsinki, Finland  
`ravantti@cs.Helsinki.FI`

**Abstract.** Cryo-electron microscopy has recently been recognized as a useful alternative to obtain three-dimensional density maps of macromolecular complexes, especially when crystallography and NMR techniques fail. The three-dimensional model is constructed from large collections of cryo-electron microscopy images of identical particles in random (and unknown) orientations.

The major problem with cryo-electron microscopy is that the images are very noisy as the signal-to-noise ratio can be below one. Thus, standard filtering techniques are not directly applicable. Traditionally, the problem of immense noise in the cryo-electron microscopy images has been tackled by clustering the images and computing the class averages. However, then one has to assume that the particles have only few preferred orientations. In this paper we propose a sound method for denoising cryo-electron microscopy images using their Radon transforms. The method assumes only that the images are from identical particles but nothing is assumed about the orientations of the particles. Our preliminary experiments show that the method can be used to improve the image quality even when the signal-to-noise ratio is very low.

## 1 Introduction

Structural biology studies how biological systems are built. Especially, determining three-dimensional electron density maps of macromolecular complexes, such as proteins or viruses, is one of the most important tasks in structural biology [1,2].

Standard techniques to obtain three-dimensional density maps of such particles (at atomic resolution) are by X-ray diffraction (crystallography) and by nuclear magnetic resonance (NMR) studies. However, X-ray diffraction requires that the particles can form three-dimensional crystals and the applicability of NMR is limited to relatively small particles [3]. There are many well-studied viruses that do not seem to crystallize and are too large for NMR techniques.

A more flexible way to reconstruct density maps is offered by cryo-electron microscopy [2,4]. Currently, the resolution of the cryo-electron microscopy reconstruction is not quite as high as resolutions obtainable by crystallography or NMR but it is improving steadily. Reconstruction of density maps by cryo-electron microscopy consists of the following subtasks:

**Specimen preparation.** A thin layer of water containing a large number of identical particles of interest is rapidly plunged into liquid ethane to freeze the specimen very quickly. Quick cooling prevents water from forming regular structures [2]. Moreover, the particles get frozen in random orientations in the iced specimen.

**Electron microscopy.** The electron microscope produces a projection of the iced specimen. This projection is called a *micrograph*. Unfortunately the electron beam of the microscope rapidly destroys the specimen so getting (multiple) accurate pictures from it is not possible.

**Particle picking.** Individual projections of particles are extracted from the micrograph. There are efficient methods to picking the projections, see e.g. [5,6].

**Orientation search.** The orientations (i.e., the projection directions for each extracted particle) for the projections are determined. There are several (heuristic) approaches for finding the orientations, see e.g. [7,8,9,10,11,12].

**Reconstruction.** If the orientations for the projections are known then quite standard tomography techniques can be applied to reconstruct the three-dimensional electron density map from the projections [2].

A main difficulty in cryo-electron microscopy is the very low signal-to-noise-ratio of the images. Thus, standard filtering techniques are not directly applicable since they filter also too much of the signal. Currently the high noise level is reduced by clustering the images to few clusters and computing class averages of the images [2]. Unfortunately, by doing that it is implicitly assumed that most of the particles are in few preferred orientations. Also, already relatively small variations in orientations make the class averages blurred.

In this paper we propose an alternative denoising method that does not assume anything about the projection directions. The method is based on some special properties of sinograms obtained from the (two-dimensional) projections of the same (three-dimensional) density map. The experiments show that it can be used to denoise even very noisy projections.

This paper is organized as follows. In Section 2 we define some central concepts of this work, in Section 3 we describe our denoising approach and in Section 4 we present some preliminary denoising experiments on simulated data. Section 5 is a short conclusion.

## 2 Projections and Sinograms

A *density map* is a mapping  $D : \mathbb{R}^3 \rightarrow \mathbb{R}$  with a compact support. An *orientation*  $o$  is a rotation of the three-dimensional space and it can be described, e.g., by a

three-dimensional rotation matrix. A *projection*  $p$  of a three-dimensional density map  $D$  to orientation  $o$  is the integral

$$p(x, y) = \int_{-\infty}^{\infty} D \left( R_o [x, y, z]^T \right) dz$$

where  $R_o$  is a rotation matrix, i.e., the mass of  $D$  is projected on a plane passing through the origin and determined by the orientation  $o$ . Some examples of projections from a density map used in our experiments (presented in Section 4) are shown in Figure 1. The brightness of a pixel is proportional to its mass.

The (three-dimensional) *Radon transform*  $\hat{D}$  of the density map  $D$  is the mapping

$$\hat{D}(x, o) = \int_{-\infty}^{\infty} \int_{-\infty}^{\infty} D \left( R_o [x, y, z]^T \right) dydz,$$

i.e.,  $\hat{D}$  consists of all one-dimensional projections of  $D$ . Similarly, the (two-dimensional) Radon transform of the projection  $p$  is the mapping

$$\hat{p}(x, \alpha) = \int_{-\infty}^{\infty} p \left( R_\alpha [x, y]^T \right) dy$$

where  $R_\alpha$  a two-dimensional rotation matrix with rotation angle  $\alpha$ .

Any two projections  $p_i$  and  $p_j$  from the same density map have a desirable property: their Radon transforms  $\hat{p}_i$  and  $\hat{p}_j$  have one (one-dimensional) common projection, a *common line*, i.e., there are  $\alpha_i$  and  $\alpha_j$  such that  $\hat{p}_i(x, \alpha_i) = \hat{p}_j(x, \alpha_j)$  for all  $x$ . This fact is known as the *Common Line Theorem* and it forms the central part of several orientation search techniques [9,10,13,14,15,16,17]. Unfortunately, the robust behavior of the orientation search methods requires that the the images are not too noisy. The recent results on the computational complexity of orientation search indicate that there is not much hope to a robust determination of orientations without considerable reduction of noise [18]. The standard approach to noise reduction in cryo-electron microscopy is to cluster the images and to compute the class averages [2]. However, this solution implicitly assumes that majority of imaging directions cluster well. In Section 3 we show how noise levels of cryo-electron microscopy images can be reduced without assuming the clusterability of the imaging directions.

In practice, a discrete versions of two-dimensional Radon transforms, called *sinograms*, are used instead of the continuous Radon transforms. A sinogram of an  $m \times m$  image is an  $l \times m$  matrix of rational numbers such that each row  $i = 1, \dots, l$  in the sinogram corresponds to one one-dimensional projection of the image to direction determined by the angle  $(i - 1)\pi/l$ . Some examples of sinograms are shown in Figure 1. There are several efficient methods for computing sinograms [19,20,21].

### 3 Sinogram Denoising

According to the Common Line Theorem, for each two projections  $p_i$  and  $p_j$  there are angles  $\alpha_i$  and  $\alpha_j$  such that  $\hat{p}_i(x, \alpha_i) = \hat{p}_j(x, \alpha_j)$  for all  $x$ . Due to

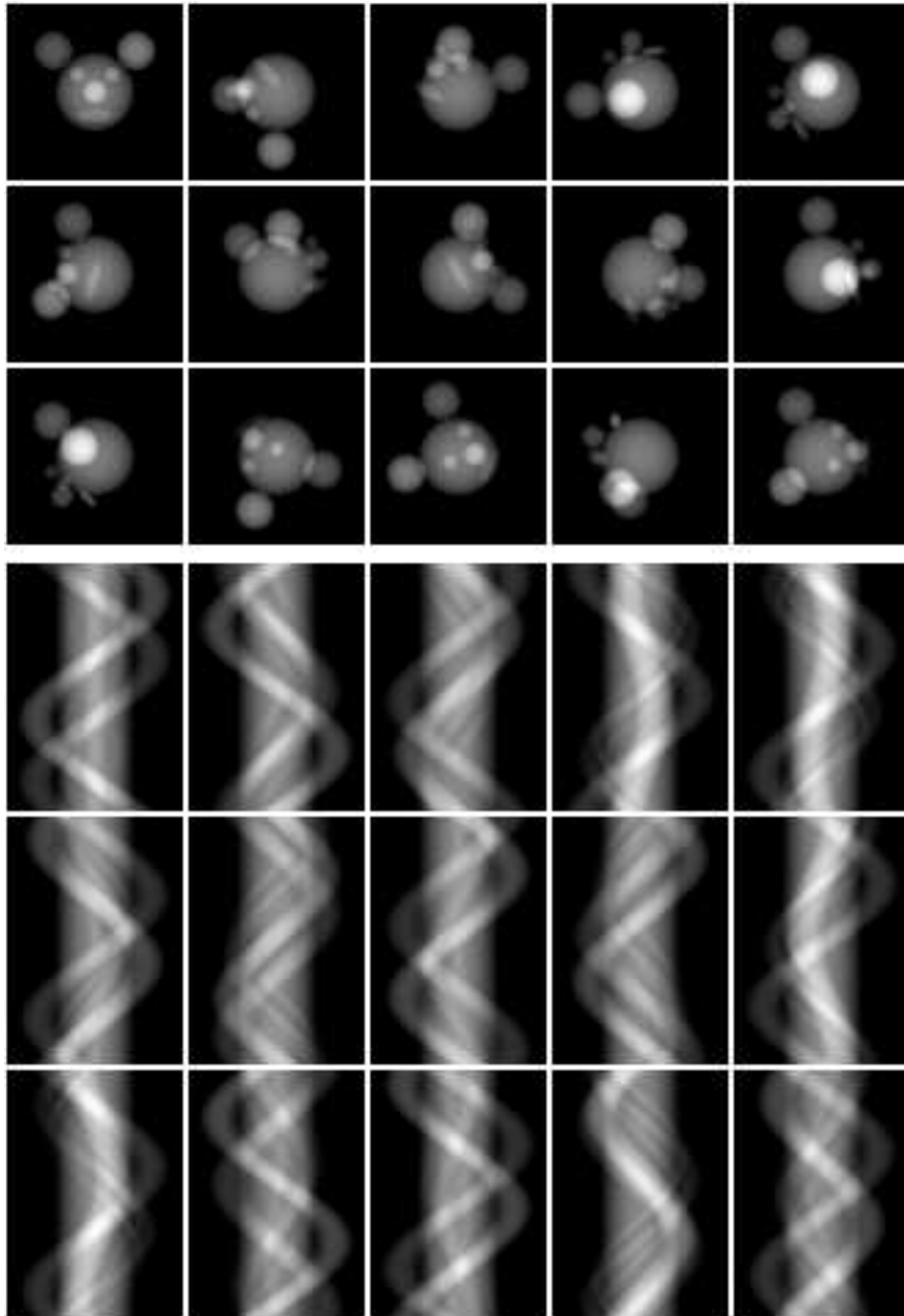


**Fig. 1.** Noiseless projections (top) of the density map from random directions and their sinograms (bottom).

discretization errors and high level of noise in cryo-electron microscopy images, the images of identical macromolecular complexes satisfy the theorem only approximately: the sinogram rows  $k_i$  and  $k_j$  corresponding to the true common line between projections  $\hat{p}_i$  and  $\hat{p}_j$  should be quite similar in the sinograms  $s_i$  of  $p_i$  and  $s_j$  of  $p_j$  if the noise level is not too high. Thus, the most similar sinogram rows in the sinograms  $s_i$  and  $s_j$  are good candidates to determine the common line between the projections  $p_i$  and  $p_j$ .

The standard approach to reduce the noise in cryo-electron microscopy images is to compute averages of several images. The same idea of computing averages can be exploited also without assuming the clusterability of the projection directions since there is always a common line between each two sinograms  $s_i$  and  $s_j$  of projections  $p_i$  and  $p_j$  of the same density map  $D$ . Thus, if  $k_i$  and  $k_j$  are the indices of the sinograms  $s_i$  and  $s_j$  corresponding to the common line between  $p_i$  and  $p_j$ , the sinogram rows  $s_i[k_i]$  and  $s_j[k_j]$  can be replaced by  $(s_i[k_i] + s_j[k_j]) / 2$ .

In general, when there are  $n$  projections from the same particle, a sinogram row  $s_i[k_i]$  can be replaced by  $\sum_{j=1}^n s_j[k_j] / n$  where the sinogram rows  $s_j[k_j]$  correspond to the common lines with  $s_i[k_i]$ .

The method is described more precisely by Algorithm 1. The algorithm inputs  $n$  sinograms  $s_1, \dots, s_n$  of size  $l \times m$  and outputs their denoised versions  $t_1, \dots, t_n$ .

---

**Algorithm 1** Sinogram denoising algorithm.

---

```

1: function DENOISE-SINOGRAMS( $s_1, \dots, s_n$ )
2:   for  $i = 1, \dots, n$  do
3:      $t_i \leftarrow s_i$ ;    $c_i \leftarrow 1$ 
4:   end for
5:   for  $i = 1, \dots, n - 1$  do
6:     for  $j = i + 1, \dots, n$  do
7:       Find the most similar sinogram lines  $s_i[k_i]$  and  $s_j[k_j]$  from  $s_i$  and  $s_j$ .
8:        $t_i[k_i] \leftarrow t_i[k_i] + s_j[k_j]$ ;    $c_i[k_i] \leftarrow c_i[k_i] + 1$ 
9:        $t_j[k_j] \leftarrow t_j[k_j] + s_i[k_i]$ ;    $c_j[k_j] \leftarrow c_j[k_j] + 1$ 
10:    end for
11:  end for
12:  for  $i = 1, \dots, n$  do
13:    for  $k = 1, \dots, l$  do
14:       $t_i[k] \leftarrow t_i[k] / c_i[k]$ 
15:    end for
16:  end for
17:  return  $t_1, \dots, t_n$ 
18: end function

```

---

Clearly, the effectiveness of this method depends on how well we are able to detect the (almost) true common lines between the sinograms of the projections. In the next section we experiment the method using correlation as the measure of the similarity between the rows.

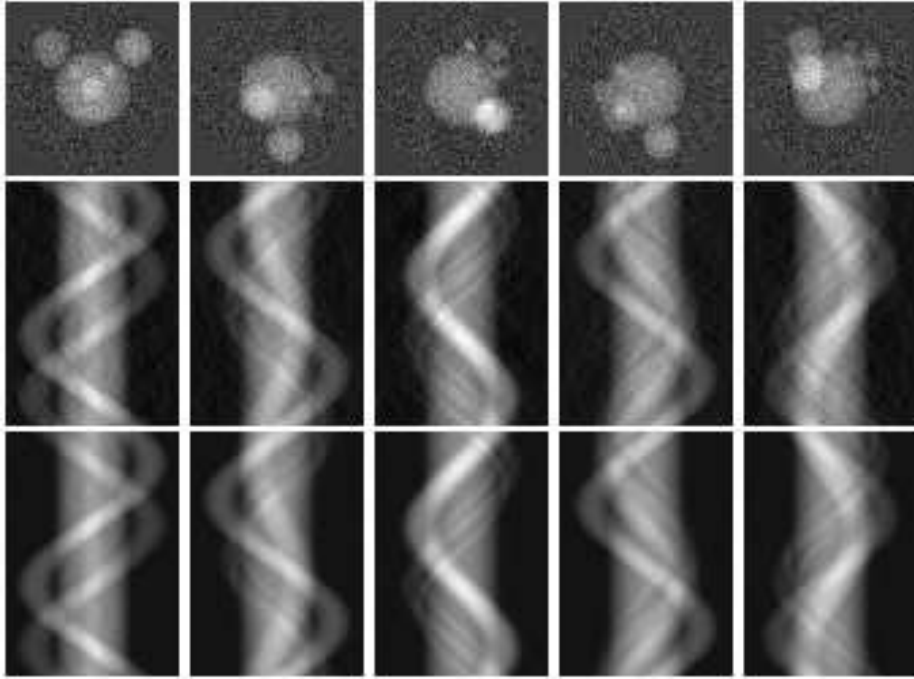


**Fig. 2.** Projections with signal-to-noise ratio 2 (top), noisy sinograms (middle) and denoised sinograms (bottom).

## 4 Experiments

We tested the effectiveness of the proposed denoising scheme with an artificial density map of size  $64 \times 64 \times 64$  voxels. The density map consists of balls with different weights, radii and locations. We projected the density map to 6300 random directions, computed sinograms of these projections, added to the projections Gaussian noise with different variances, and computed the sinograms of noiseless and noisy projections (see Figure 1 and Figures 2–5, respectively) with angular step-size of 4 degrees. Furthermore, we denoised the sinograms of the noisy projections using the proposed denoising method. The similarity measure used between the sinogram rows was the correlation coefficient.

The results are shown in Figures 2, 3, 4, and 5. Denoising seems to work reasonably well, at least visually. Twilight zone of the straightforward implementation of the method is between signal-to-noise ratios 0.5 and 0.3. Note that the low contrast of the sinograms in Figure 5 is due to the normalization of intensity values.

To get more quantitative information about our denoising method, we computed correlation coefficients between noiseless, noisy and denoised sinograms with different signal-to-noise ratios. The results are shown in Table 1.

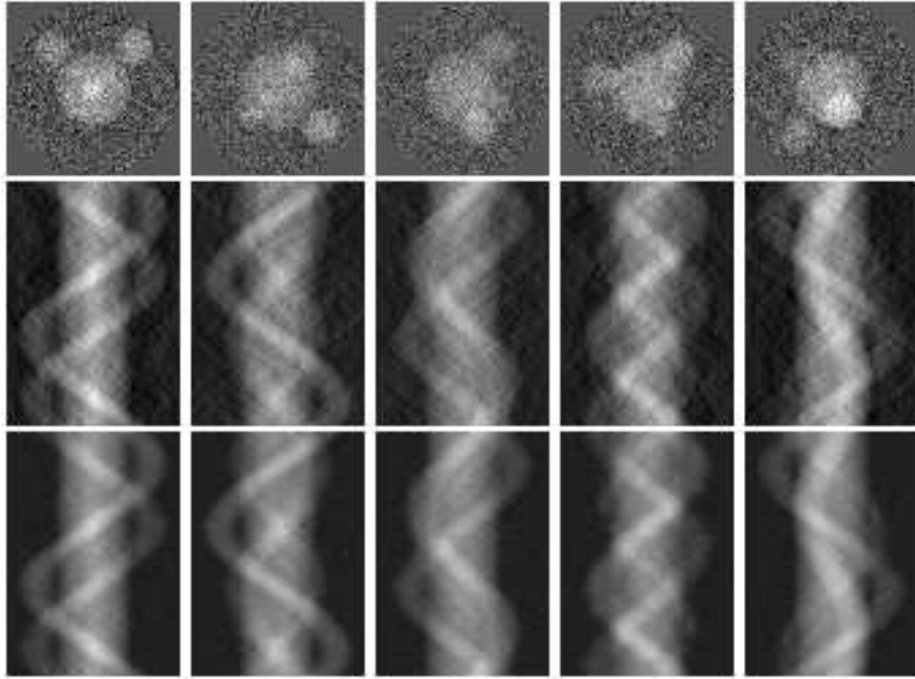


**Fig. 3.** Projections with signal-to-noise ratio 1 (top), noisy sinograms (middle) and denoised sinograms (bottom).

**Table 1.** Correlations between noiseless, noisy and denoised sinograms.

signal-to-noise ratio	noiseless vs. noisy		noiseless vs. denoised		noisy vs. denoised	
	mean	variance	mean	variance	mean	variance
2	0.9962	1.293e-07	0.9997	5.303e-09	0.9970	7.805e-08
1	0.9851	2.225e-06	0.9971	5.264e-07	0.9910	7.813e-07
0.5	0.9437	4.318e-05	0.9800	3.665e-05	0.9747	1.341e-05
0.3	0.8846	6.772e-04	0.8512	1.450e-02	0.8630	1.123e-02

Clearly, the sinogram denoising improved the correlation coefficients also in this experiment, although the method did not show improvement with respect to average of the correlation coefficient with signal-to-noise ratio 0.3. Note that although all correlations are quite high, the correlations are order of magnitude closer to the maximum correlation (i.e., correlation 1) for all signal-to-noise ratios except the signal-to-noise ratio 0.3.

Overall, the results are very promising, especially as the implementation used in the experiments is a straightforward implementation of Algorithm 1; for example, no additional filtering nor more sophisticated estimation of sinogram row similarities were used.

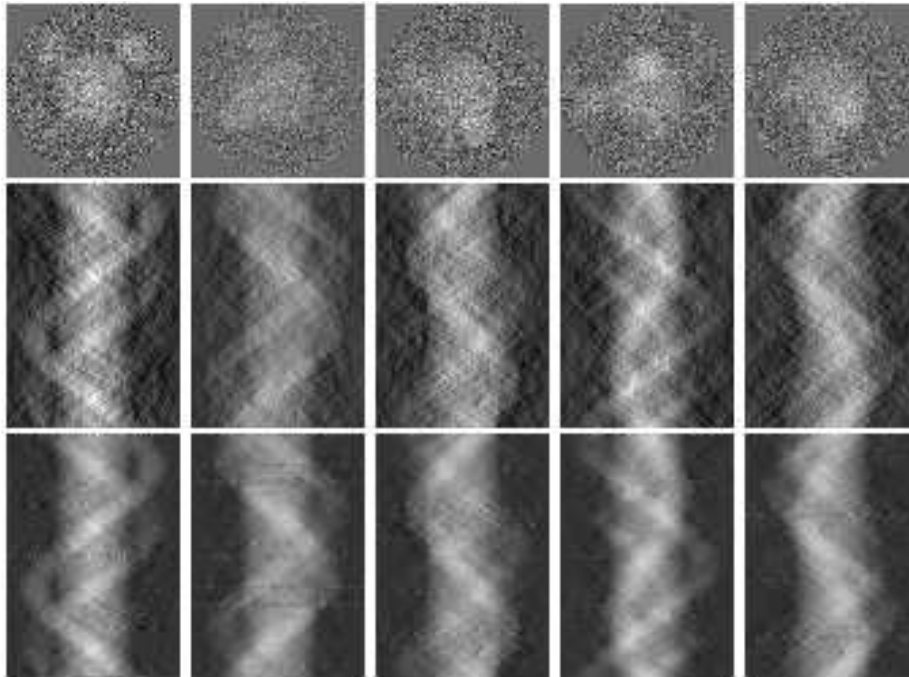


**Fig. 4.** Projections with signal-to-noise ratio 0.5 (top), noisy sinograms (middle) and denoised sinograms (bottom).

## 5 Conclusions

In this paper, we proposed a novel denoising method for cryo-electron microscopy images that, unlike the previously known approaches, does not assume anything about imaging directions of the images.

The described approach is based on denoising the sinograms of the cryo-electron microscopy images and thus it is directly applicable within several orientation search methods that determine the orientations using the pairwise similarities between sinogram rows [9,10,13,14,15,16,17]. We showed experimentally that even a straightforward implementation of the denoising approach is able to reduce noise even when the signal-to-noise ratios are very low.

Although the denoising method seems very promising, there is still plenty of room for improvements. The effectiveness of the method relies on reasonably robust common line detection which could clearly be improved. For example, as the common lines fix the relative orientations of the cryo-electron microscopy images, these constraints could be used to expose false common lines. Furthermore, the possible information about symmetry could be used to improve the signal-to-noise ratio. As future work we plan to study the improvements suggested above and other heuristics to further facilitate the effectiveness of the

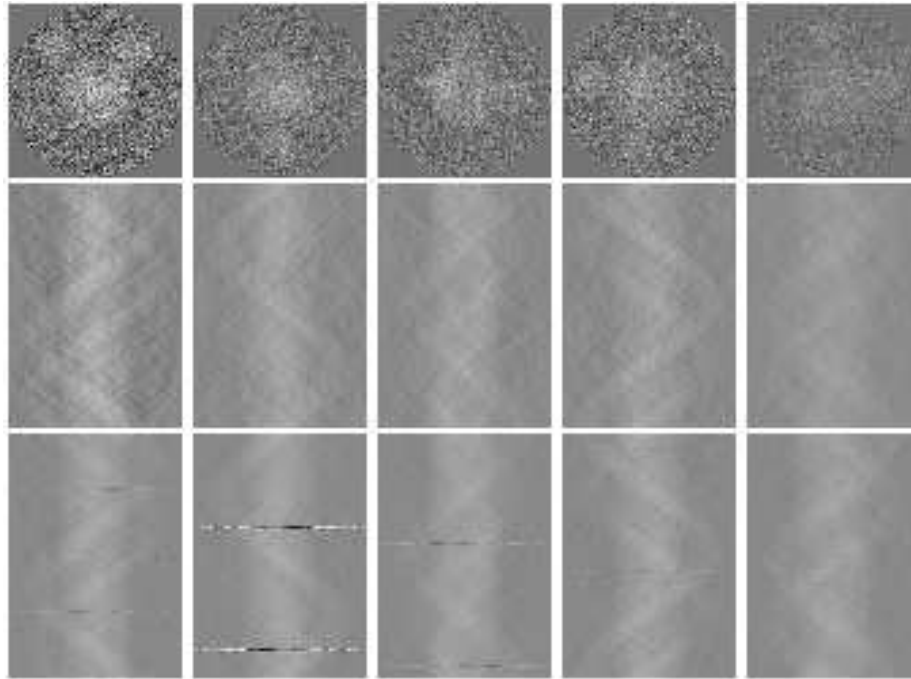


**Fig. 5.** Projections with signal-to-noise ratio 0.3 (top), noisy sinograms (middle) and denoised sinograms (bottom).

sinogram denoising approach proposed in this paper. Also, more sophisticated methods to evaluate the success of the denoising shall be investigated. The quality of the reconstruction of the density map depends also on the reconstruction method. Thus, the suitability of different reconstruction algorithms to be used in conjunction with the sinogram denoising is also of our interest.

**Acknowledgements** We wish to thank Dennis Bamford, Teemu Kivioja and Esko Ukkonen for helpful discussions on sinograms and cryo-electron microscopy.

## References

1. Baker, T.S., Olson, N.H., Fuller, S.D.: Adding the third dimension to virus life cycles: Three-dimensional reconstruction of icosahedral. *Microbiology and Molecular Biology Reviews* **63** (1999) 862–922
2. Frank, J.: *Three-Dimensional Electron Microscopy of Macromolecular Assemblies*. Academic Press (1996)
3. Carazo, J.M., Sorzano, C.O., Rietzel, E., Schröder, R., Marabini, R.: Discrete tomography in electron microscopy. In Herman, G.T., Kuba, A., eds.: *Discrete*

- Tomography: Foundations, Algorithms, and Applications. Applied and Numerical Harmonic Analysis. Birkhäuser (1999) 405–416
4. Crowther, R., DeRosier, D., Klug, A.: The reconstruction of a three-dimensional structure from projections and its application to electron microscopy. *Proceedings of the Royal Society of London A* **317** (1970) 319–340
  5. Kivioja, T., Ravantti, J., Verkhovskiy, A., Ukkonen, E., Bamford, D.: Local average intensity-based method for identifying spherical particles in electron micrographs. *Journal of Structural Biology* **131** (2000) 126–134
  6. Nicholson, W.V., Glaeser, R.M.: Review: Automatic particle detection in electron microscopy. *Journal of Structural Biology* **133** (2001) 90–101
  7. Baker, T.S., Cheng, R.H.: A model-based approach for determining orientations of biological macromolecules imaged by cryoelectron microscopy. *Journal of Structural Biology* **116** (1996) 120–130
  8. Doerschuk, P.C., Johnson, J.E.: *Ab initio* reconstruction and experimental design for cryo electron microscopy. *IEEE Transactions on Information Theory* **46** (2000) 1714–1729
  9. Fuller, S.D., Butcher, S.J., Cheng, R.H., Baker, T.S.: Three-dimensional reconstruction of icosahedral particles – the uncommon line. *Journal of Structural Biology* **116** (1996) 48–55
  10. van Heel, M.: Angular reconstitution: a posteriori assignment of projection directions for 3D reconstruction. *Ultramicroscopy* **21** (1987) 11–124
  11. Ji, Y., Marinescu, D.C., Chang, W., Baker, T.S.: Orientation refinement of virus structures with unknown symmetry. In: *Proceedings of the International Parallel and Distributed Processing Symposium*. IEEE Computer Society (2003) 49–56
  12. Lanczycki, C.J., Johnson, C.A., Trus, B.L., Conway, J.F., Steven, A.C., Martino, R.L.: Parallel computing strategies for determining viral capsid structure by cryoelectron microscopy. *IEEE Computational Science & Engineering* **5** (1998) 76–91
  13. Bellon, P.L., Cantele, F., Lanzavecchia, S.: Correspondence analysis of sinogram lines. Sinogram trajectories in factor space replace raw images in the orientation of projections of macromolecular assemblies. *Ultramicroscopy* **87** (2001) 187–197
  14. Bellon, P.L., Lanzavecchia, S., Scatturin, V.: A two exposures technique of electron tomography from projections with random orientation and a *quasi*-Boolean angular reconstitution. *Ultramicroscopy* **72** (1998) 177–186
  15. Lauren, P.D., Nandhakumar, N.: Estimating the viewing parameters of random, noisy projections of asymmetric objects for tomographic reconstruction. *IEEE Transactions on Pattern Analysis and Machine Intelligence* **19** (1997) 417–430
  16. Penczek, P.A., Zhu, J., Frank, J.: A common-lines based method for determining orientations for  $N > 3$  particle projections simultaneously. *Ultramicroscopy* **63** (1996) 205–218
  17. Thuman-Commike, P.A., Chiu, W.: Improved common line-based icosahedral particle image orientation estimation algorithms. *Ultramicroscopy* **68** (1997) 231–255
  18. Mielikäinen, T., Ravantti, J., Ukkonen, E.: The computational complexity of orientation search in cryo-electron microscopy. In Bubak, M., van Albada, G.D., Sloat, P.M.A., Dongarra, J.J., eds.: *Computational Science – ICCS 2004*. Volume 3036 of *Lecture Notes in Computer Science*. Springer-Verlag (2004)
  19. Brady, M.L.: A fast discrete approximation algorithm for the Radon transform. *SIAM Journal on Computing* **27** (1998) 107–119
  20. Brandt, A., Dym, J.: Fast calculation of multiple line integrals. *SIAM Journal on Computing* **20** (1999) 1417–1429
  21. Lanzavecchia, S., Tosoni, L., Bellon, P.L.: Fast sinogram computation and the sinogram-based alignment of images. *Cabios* **12** (1996) 531–537